INTERNATIONAL JOURNAL FOR NUMERICAL METHODS IN FLUIDS
Int. J. Numer. Meth. Fluids 2004; **45**:301–319 (DOI: 10.1002/fld.699)

Static wetting on flexible substrates: a finite element formulation

Srinath Madasu and Richard A. Cairncross*,†

Department of Chemical Engineering, Drexel University, Philadelphia, PA 19104, U.S.A.

SUMMARY

In static wetting on an elastic substrate, force exerted by the liquid–vapour surface tension on a solid surface deforms the substrate, producing a capillary ridge along the contact line. This paper presents a finite element formulation for predicting elastic deformation, close to the static wetting line (with angle of contact $= 90^\circ$ and $\sigma_{SV} = \sigma_{SL}$). The substrate deformation is modelled with the Mooney–Rivlin constitutive law for incompressible rubber-like solids.

At the contact line, a stress singularity is known to arise, due to the surface tension acting on a line of infinitesimal thickness. To relive the stress singularity, either (i) the surface tension is applied over a finite contact region (of macroscopic thickness), or (ii) the solid crease angle is fixed. These two options suggest that normal component of Neumann's triangle law of forces, for the three surface tensions, is not applicable for elastic substrates (as for rigid ones). The vertical displacement of the contact line is a strong function of liquid/vapour surface tension and shear modulus of the solid. Copyright © 2004 John Wiley & Sons, Ltd.

KEY WORDS: static wetting; flexible substrate; pseudo-solid mesh motion; finite element; Young's equation; Neumann's triangle; crease angle; line force; singularity; capillarity

1. INTRODUCTION

Wetting is the process of displacing a vapour by a liquid, on a solid surface with the *contact line* the line of intersection of solid, liquid and vapour phases [1, 2]. If neither the solid nor the contact line is moving, wetting is called static. Under equilibrium conditions, static wetting on a rigid solid involves the balance of three surface tension forces arising at the contact line. Young's equation is derived from a balance of forces parallel to the solid surface, and relates the contact angle to the surface tensions:

$$\cos\theta = \frac{\sigma_{SV} - \sigma_{SL}}{\sigma_{LV}} \tag{1}$$

*Correspondence to: R. A. Cairncross, Department of Chemical Engineering, Drexel University, Philadelphia, PA 19104, U.S.A.
†E-mail: cairncro@coe.drexel.edu

Contract/grant sponsor: Sandia National Laboratories

Received 11 April 2003
Revised 5 January 2004

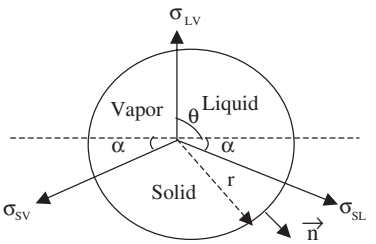

Figure 1. Force balance around the contact line, on a control volume of radius r with unit normal $\vec{\mathbf{n}}$ to the surface. The dashed line represents the solid surface, before deformation.

where θ is the contact angle [3], and, σ_{SL}, σ_{SV} and σ_{LV} are the solid/liquid, solid/vapour and liquid/vapour surface tensions, respectively.

In addition to these three surface tensions, the elastic forces in the solid enter the force balance at the static wetting line, for flexible solids.Figure 1 shows a control volume for balancing forces at a wetting line:

$$\cos\theta\sigma_{LV} = \cos\alpha(\sigma_{SV} - \sigma_{SL}) - f_{st} \quad \text{(tangential component)} \tag{2a}$$

$$\sin\theta\sigma_{LV} = \sin\alpha(\sigma_{SV} + \sigma_{SL}) - f_{sn} \quad \text{(normal component)} \tag{2b}$$

where θ and α are defined in Figure 1 (the dashed line shows a bisecting plane that is defined such that the angle α is the same for the solid/vapour and the solid/liquid surfaces), f_{st} and f_{sn} are, respectively, the tangential and normal components of the elastic force. In a rigid solid, $\alpha = 0$, $f_{st} = 0$, Equation (2a) or (1) is the tangential component of Neumann's triangle law of forces, and the normal component of the liquid–vapour surface tension is balanced by the normal component of the elastic force, (Equation (2b)). In a flexible solid, the liquid–vapour surface tension is balanced by both elastic force and solid surface tensions.

Several researchers [3–9] predicted substrate deformation near a static wetting line. Lester [3] considered a weightless drop on a semi-infinite solid and assumed a uniform normal pressure in the interface layer, which he considered to be of molecular dimensions. Lester showed that α depends on both the liquid/vapour surface tension and the modulus of the solid. Rusanov [4] used a similar approach to calculate the displacement field, for a drop resting on a flexible solid, but he included tangential interfacial stresses and gravity. Rusanov showed that there is a kink at the contact line. Fortes [5] used the balance of surface tension and pressure forces, for a weightless drop on a membrane, to obtain a relationship between the contact angle and the surface tensions. Shanahan [6] used a balance of free energy, including gravity, for a drop on a thin plate or a membrane, to obtain force balances at the static contact line. He did not calculate the shapes of the drop and the solid. Kern and Muller [7] followed the same approach, for a drop on a thin elastic solid, to solve for drop and solid profiles. Olives [8, 9] used a thermodynamic approach for obtaining equilibrium equations of capillarity and elasticity, including gravity, for a drop on a thin plate, in which he not only included bending but also stretching of plate, which was neglected by the previous researchers. He showed that discontinuities in the elastic displacements arise at the contact line and showed that

Young's equation of force balance is not valid for flexible solids. In this paper, a novel approach using numerical solution by the finite element method is used to model static wetting on flexible substrates, with non-linear large strain elasticity and finite substrate thickness. The numerical solution suggests that normal component of Neumann's triangle law of forces, for the three surface tensions, is not valid for flexible solids (as for rigid ones).

For deformable solids, a singularity arises at the contact line, due to the line force, which results in infinite displacement. In order to relieve this singularity in numerical predictions of elastic deformation near a contact line, two conditions are considered, in this paper:

- Applying the line force over a finite contact region.
- Applying a crease angle condition at the contact line.

The first condition (which results in finite displacement) is based on the fact that surface tension force acts over a finite contact region of molecular dimensions, and not at a line. The second condition, by its geometrical nature, also leads to a finite displacement. In numerical predictions, the finite contact region arises from the discretization—i.e. size of the elements adjacent to the contact line. An analytical model for finite displacement, due to a distributed force over a finite contact region, is also presented in this paper. This option has been extended for modelling dynamic wetting on flexible substrates [10].

These physical considerations are elaborated upon in the first section of the paper. The second section of the paper describes the model formulation, the boundary conditions applied to the momentum equations and the mesh motion scheme, for the test case. The third section describes the finite element formulation, application of boundary conditions, method of solving the non-linear equations and mesh refinement studies. The fourth section discusses the finite element solution, the analytical model for a distributed force at the contact line, and the results from applying the crease angle condition and the distributed line force condition.

2. PHYSICAL THEORY OF STATIC WETTING ON FLEXIBLE SUBSTRATES

2.1. Model formulation

The model formulation for static wetting on flexible substrates is applied to a liquid contained between two flexible plates. The system analysed consists of a 2D deformable planar elastomeric slot, as shown in Figure 2(a), which is attached to a rigid solid and immersed in a liquid. The wetting liquid rises up in the gap between the two solids and achieves an equilibrium state of static wetting. The flexible solid, with assumed negligible body forces, deforms under the action of capillary pressures at the solid/vapour and solid/liquid surfaces, and surface tension forces at the wetting line (hydrostatic pressures being neglected). By symmetry, only one of the two solids needs to be analysed (Figure 2(b)).

In the solid domain, the displacement field is described by Cauchy's equilibrium equation. This equation can be written in dimensionless form, in the Eulerian reference frame, as follows:

$$\nabla \cdot \mathbf{T}_S = 0 \tag{3}$$

where $\mathbf{T}_S$ is the dimensionless stress tensor (stress tensor divided by the shear modulus G). The Mooney–Rivlin constitutive law [11] is used as the stress–strain relationship for a

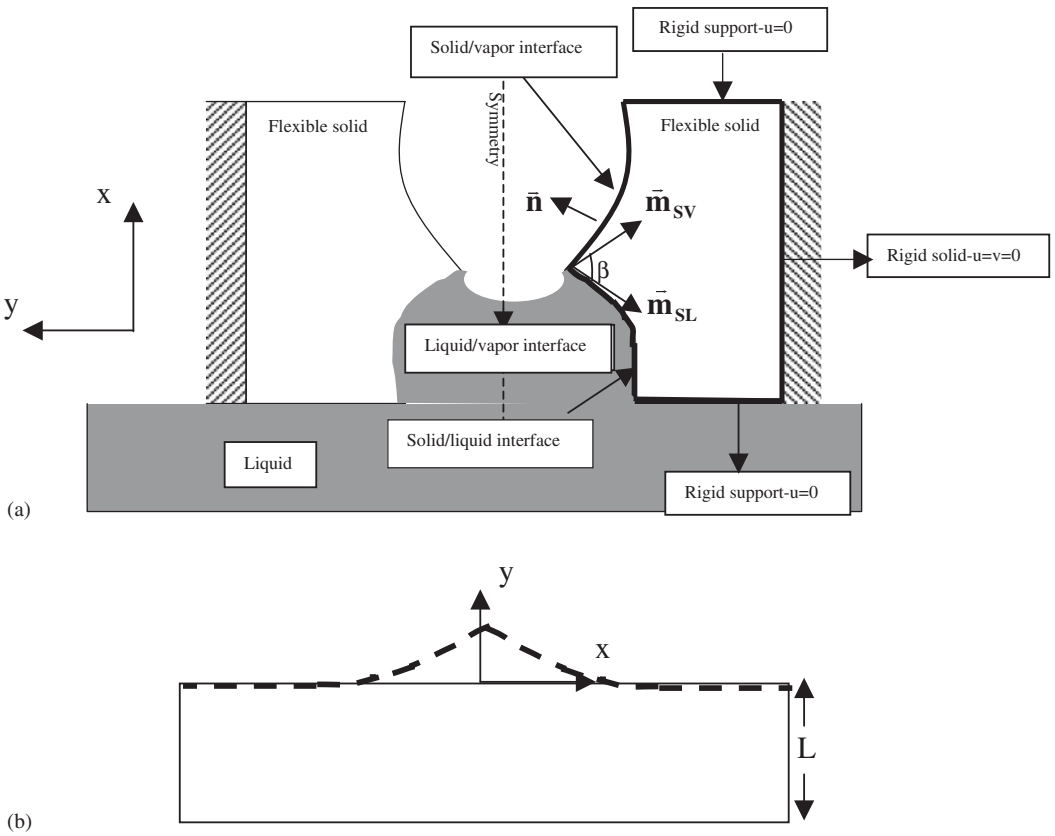

Figure 2. (a) Model formulation of static wetting, for a liquid between two capillary flexible plates. β is the crease angle. Other parameters are defined in the paper. (b) Computational domain, where L is the thickness of the solid.

rubber-like solid:

$$\mathbf{T}_S = (-p_s - 2fG + G)\mathbf{I} + f\mathbf{B} - (1-f)\mathbf{B}^{-1} \tag{4}$$

which contains the isotropic pressure term (divided by G) and the stress term resulting from the deformation, $\mathbf{I}$ is the identity tensor, f a constant ranging between 0 and 1, and $\mathbf{B} = \mathbf{F}\mathbf{F}^{\mathrm{T}}$ the left Cauchy–Green deformation tensor. By setting $f = 1$, the neo-Hookean constitutive law is obtained from Mooney–Rivlin constitutive law. Since the problem is two-dimensional, the deformation gradient tensor, $\mathbf{F}$, is given as follows in terms of the displacements u (x-component) and v (y-component), in deformed co-ordinates:

$$\mathbf{F} = \begin{bmatrix} 1 - \dfrac{\partial v}{\partial y} & \dfrac{\partial u}{\partial y} \\ \dfrac{\partial v}{\partial x} & 1 - \dfrac{\partial u}{\partial x} \end{bmatrix} \tag{5}$$

Since the solid is incompressible, a constant, $-(2f-1)\mathbf{I}$, needs to be added to the above constitutive law, in order to make the solid stress go to zero when the displacement goes to zero.

The conservation of volume in the solid is expressed by

$$|\mathbf{F}| = \det \mathbf{F} = 1 \tag{6}$$

This completes the formulation of field equations of the test problem. Boundary conditions are needed to solve the above model, which include momentum balances along the solid/liquid and solid/vapour interfaces, boundary conditions on the other solid boundaries, as shown in Figure 2(a), and the boundary conditions at the contact line. The boundary conditions and the mesh motion scheme are discussed in the following sections.

2.2. Boundary conditions

Along the solid/vapour and solid/liquid interfaces, the stress is assumed to be normal to the surface (i.e. $\vec{\mathbf{n}} \cdot \mathbf{T}_s$ is parallel to $\vec{\mathbf{n}}$) and the boundary condition balances the normal stress in the solid, external pressure and surface tension in the interface (Laplace equation, as for a fluid/fluid interface). The external pressure p_{ext} is assumed to be zero (in the liquid and in the vapour).

solid/vapour interface:

$$-\vec{\mathbf{n}} \cdot \mathbf{T}_S = \vec{\mathbf{n}} \cdot p_{ext}\mathbf{I} + \frac{2H\vec{\mathbf{n}}}{\mathbf{Ca}_{ESV}}; \quad \mathbf{Ca}_{ESV} = \frac{GL}{\sigma_{SV}} \tag{7}$$

solid/liquid interface:

$$-\vec{\mathbf{n}} \cdot \mathbf{T}_S = \vec{\mathbf{n}} \cdot p_{ext}\mathbf{I} + \frac{2H\vec{\mathbf{n}}}{\mathbf{Ca}_{ESL}}; \quad \mathbf{Ca}_{ESL} = \frac{GL}{\sigma_{SL}} \tag{8}$$

where $\vec{\mathbf{n}}$ is the outer normal to the solid, L is the thickness of the solid domain, H is the surface mean curvature (multiplied by L; $H<0$ if the solid surface is concave), $\mathbf{Ca}_{ESV}$ and $\mathbf{Ca}_{ESL}$ are the solid/vapour or solid/liquid elastic capillary numbers, respectively, σ_{SV} and σ_{SL} the solid/vapour and solid/liquid surface tensions, respectively. The elastic capillary numbers scale the significance of the elastic forces in the solid to the surface tensions.

2.3. Force balance at the contact line

The forces acting in the vicinity of the contact line are balanced over a circular-shaped control volume, as shown in Figure 1. Assuming negligible pressures in the gas and liquid phases, the three surface tensions which act tangent to the interfaces and the stress from the solid enter the force balance. By shrinking the pillbox, i.e. as r tends to zero, the force balance for static wetting takes the following form:

$$\mathbf{f}_s + \vec{\mathbf{m}}_{LV}\sigma_{LV} + \vec{\mathbf{m}}_{SV}\sigma_{SV} + \vec{\mathbf{m}}_{SL}\sigma_{SL} = 0 \tag{9}$$

$$\mathbf{f}_S = \lim_{r\to 0} \int_{\theta_{SV}}^{\theta_{SL}} \vec{\mathbf{n}} \cdot \bar{\mathbf{T}}_S \mathbf{r}\, \mathrm{d}\theta \tag{10}$$

where $\mathbf{f}_s$ is the force in the solid due to elastic stress, $\bar{\mathbf{T}}_S = G\mathbf{T}_S$ is the dimensional stress tensor, $\vec{\mathbf{n}}$ is the outer normal to the control volume, θ_{SV} and θ_{SL} are the angular locations of

the solid/vapour and solid/liquid surfaces, respectively; $\vec{\mathbf{m}}_{LV}$, $\vec{\mathbf{m}}_{SV}$ and $\vec{\mathbf{m}}_{SL}$ are tangent to the liquid/vapour, solid/vapour and solid/liquid interfaces, respectively, at the contact line.

Equation (9) represents the new form of force balance at the contact line, for static wetting on flexible substrates. The singular force in the solid needs to be relieved in order to obtain a finite solution; with this aim in view, special boundary conditions at the contact line are required, as discussed in the next section.

2.4. Boundary conditions at the contact line

In this paper, the following case is used for all numerical solutions: the liquid/vapour surface tension acts along the y-direction ($\theta = 90^\circ$) and $\sigma_{SV} = \sigma_{SL}$. There are two options for applying boundary conditions at the contact line, within the numerical solution:

- *Crease angle condition*, which fixes the value of β (Figure 2(a)):

$$\vec{\mathbf{m}}_{SL} \cdot \vec{\mathbf{m}}_{SV} = \cos\beta \tag{11}$$

- *Distributed line force condition*, which considers the liquid/vapour surface tension force distributed over a finite contact region.

The crease angle condition, by its geometrical nature, leads to a finite displacement of the contact line. Applying distributed liquid/vapour surface tension force over a finite contact region also relieves the singularity, resulting in a finite displacement (see the analytical model, Section 4.2.2).

2.5. Mesh motion scheme

The mesh motion scheme used in this paper is pseudo-solid mesh motion [12–15]. This belongs to the class of ALE method, where the mesh moves independent of the underlying solid (see also Reference [10]). The nodes are moved as though they behave as an elastic solid, by solving Cauchy's equation of equilibrium subject to boundary deformation, resulting from the solution of the real solid deformation field.

2.6. Boundary conditions on the mesh

In the following, the x-direction will be called 'horizontal' and the y-direction 'vertical'. The horizontal and vertical displacements of the mesh are set to zero on the rigid support boundaries of the domain. On the rigid solid boundary, shear free boundary condition is applied on the horizontal displacement and the vertical displacement of the mesh is set equal to zero. The solid/vapour and solid/liquid free surfaces are assumed to be shear free and the vertical displacement of the mesh is set equal to the vertical displacement of the flexible solid (Lagrange mesh). At the contact line, the horizontal displacement of the mesh is set to zero and its vertical displacement is set equal to that of the solid.

3. GALERKIN FINITE ELEMENT FORMULATION

3.1. Residual calculations in the finite element method

The coupled system of equations and boundary conditions involving free surfaces is non-linear, making it difficult to get an analytical solution, and hence, the numerical finite element method (FEM) is used. FEM approximates the solution in each element to be the product of the nodal

unknowns and the basis functions. The single-phase problem in this paper requires solving for the solid displacements, mesh positions and pressure in the solid. The basis functions for the displacement and the pressure are chosen to be biquadratic and bilinear, respectively. The basis functions for pressure are of one order less than those for displacement, in order to satisfy the Ladyzhenskaya–Babuska–Brezzi (LBB) condition [16].

The displacement fields are given by

$$u = \sum_{i=1}^{n} u_i \phi_i(x, y); \quad v = \sum_{i=1}^{n} v_i \phi_i(x, y) \tag{12}$$

in which $\phi_i(x, y)$ are the biquadratic basis functions and n is the number of nodes, in an element where u and v are calculated.

Similarly, the pressure field in an element is given by

$$p_S = \sum_{i=1}^{m} p_{S_i} \psi_i(x, y) \tag{13}$$

where $\psi_i(x, y)$ are the bilinear basis functions and m is the number of nodes.

The momentum equation is weighted with the biquadratic basis function and then integrated by parts to get a weighted residual:

$$R_i^m = \int_V (\nabla \cdot \mathbf{T}_S)\phi_i \, \mathrm{d}V = -\int_V (\nabla \phi_i \cdot \mathbf{T}_S) \, \mathrm{d}V + \int_S \phi_i (\vec{\mathbf{n}} \cdot \mathbf{T}_S) \, \mathrm{d}S \tag{14}$$

The incompressibility constraint is also weighted using the bilinear basis function:

$$R_i^c = \int_V (|\mathbf{F}| - 1)\psi_i \, \mathrm{d}V = \int_V (|\mathbf{I} - \nabla \mathbf{u}|^{-1} - 1)\psi_i \, \mathrm{d}V \tag{15}$$

The second term in Equation (14) is a boundary integral, which can be evaluated from boundary conditions. For the capillary conditions (7)–(8), the boundary integral term can be expressed in terms of surface divergence [17] and added to the residual. The details of this derivation are provided in Reference [14].

3.2. *Momentum balance in the vicinity of the contact line*

The weighted residual of the momentum equation, integrated over all the elements near the contact line (see Figure 3), is

$$\int_{V_s} (\nabla \cdot \bar{\mathbf{T}}_S)\phi_{\mathrm{SCL}} \, \mathrm{d}V = 0 \tag{16}$$

where ϕ_{SCL} is the weighting function that corresponds to the node at the static contact line.

Integrating by parts, Equation (16) gives

$$\int_{V_S} (\nabla \cdot \bar{\mathbf{T}}_S)\phi_{\mathrm{SCL}} \, \mathrm{d}V = -\int_{V_S} \bar{\mathbf{T}}_S \cdot \nabla \phi_{\mathrm{SCL}} \, \mathrm{d}V + \int_S \vec{\mathbf{n}} \cdot \bar{\mathbf{T}}_S \phi_{\mathrm{SCL}} \, \mathrm{d}S \tag{17}$$

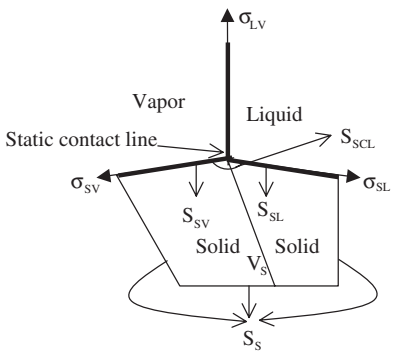

Figure 3. Balance of momentum in the vicinity of the static contact line.

where $\vec{\mathbf{n}}$ is the outer normal to V_S. The surface integral can be split into contributions from the solid/liquid and solid/vapour interfaces and from the contact line, because of singularity (see Figure 3):

$$\int_{V_S} (\nabla \cdot \bar{\mathbf{T}}_S)\phi_{SCL}\,\mathrm{d}V = -\int_{V_S} \bar{\mathbf{T}}_S \cdot \nabla\phi_{SCL}\,\mathrm{d}V + \int_{S_{SV}} \vec{\mathbf{n}} \cdot \bar{\mathbf{T}}_S \phi_{SCL}\,\mathrm{d}S + \int_{S_{SL}} \vec{\mathbf{n}} \cdot \bar{\mathbf{T}}_S \phi_{SCL}\,\mathrm{d}S + \int_{S_{SCL}} \vec{\mathbf{n}} \cdot \bar{\mathbf{T}}_S \phi_{SCL}\,\mathrm{d}S + \int_{S_S} \vec{\mathbf{n}} \cdot \bar{\mathbf{T}}_S \phi_{SCL}\,\mathrm{d}S \tag{18}$$

The last term in Equation (18) drops out because $\phi_{SCL} = 0$ along the boundary S_S. S_{SCL} represents a small patch of surface inside the solid, in the vicinity of the static contact line. The integral over S_{SCL} is equal to $-\mathbf{f}_s$, as S_{SCL} goes to zero (Equation (10) with opposite $\vec{\mathbf{n}}$). The integrals S_{SV} and S_{SL} over can be expressed, using Equations (7)–(8) and integrating by parts in terms of surface tension gradients:

$$\int_V \nabla \cdot \bar{\mathbf{T}}\phi_{SCL}\,\mathrm{d}V = -\mathbf{f}_s - \vec{\mathbf{m}}_{SV}\sigma_{SV} - \vec{\mathbf{m}}_{SL}\sigma_{SL} - \int_{V_S} \bar{\mathbf{T}}_S \cdot \nabla\phi_{SCL}\,\mathrm{d}V - \int_{S_{SL}} \sigma_{SL}\nabla_s\phi_{SCL}\,\mathrm{d}S - \int_{S_{SV}} \sigma_{SV}\nabla_s\phi_{SCL}\,\mathrm{d}S \tag{19}$$

where ∇_s is the surface gradient operator [17]. The sum of the first three terms is equal to $\vec{\mathbf{m}}_{LV}\sigma_{LV}$, according to Equation (9):

$$\int_{V_S} (\nabla \cdot \bar{\mathbf{T}}_S)\phi_{SCL}\,\mathrm{d}V = -\int_{V_S} \bar{\mathbf{T}}_S \cdot \nabla\phi_{SCL}\,\mathrm{d}V - \int_{S_{SL}} \sigma_{SL}\nabla_s\phi_{SCL}\,\mathrm{d}S - \int_{S_{SV}} \sigma_{SV}\nabla_s\phi_{SCL}\,\mathrm{d}S + \vec{\mathbf{m}}_{LV}\sigma_{LV} \tag{20}$$

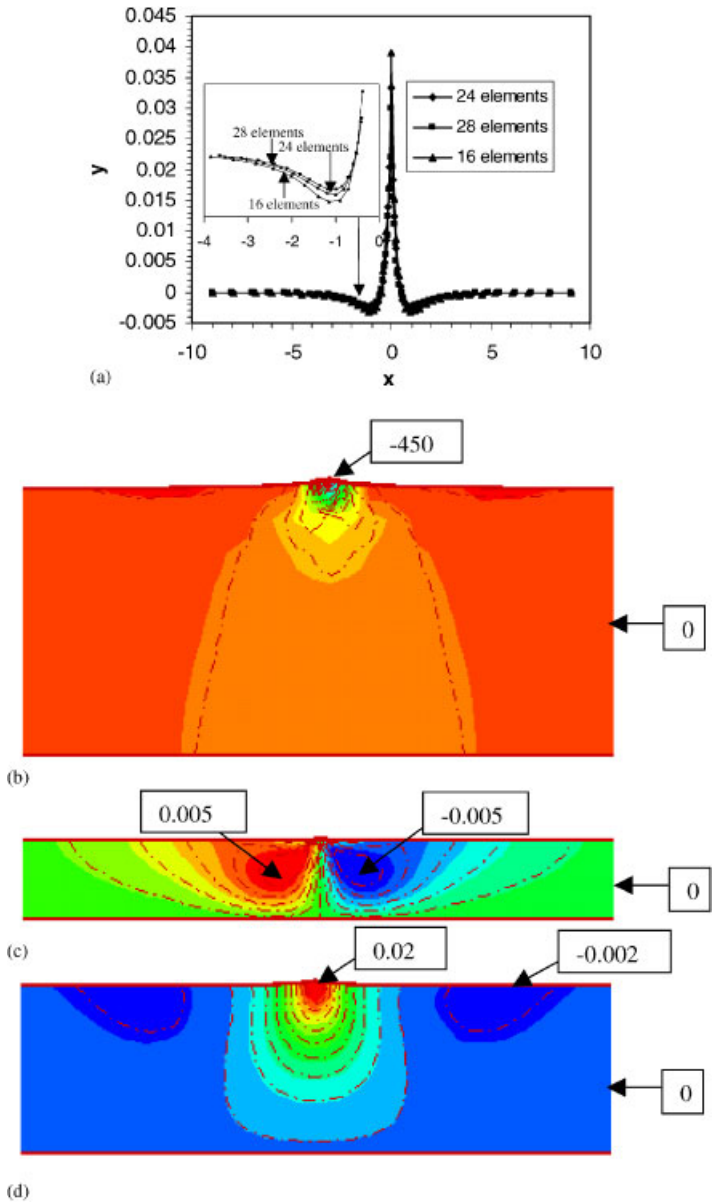

Plate 1. (a) Comparison of the free surface of the solid (co-ordinates x/L, y/L), with 16 elements, 24 elements and 28 elements (in the x-direction). Comparison of contour plots of (b) pressure, (c) horizontal displacement and (d) vertical displacement, for 24 elements (solid areas) versus 28 elements (dash–dot lines). The parameters $L_x/L = 18$, $f = 1$, crease angle condition $\beta = 150°$, and $\mathbf{Ca}_{\mathrm{ESV}} = \mathbf{Ca}_{\mathrm{ESL}} = 10$ are used for this comparison. The minimum and maximum pressure contour levels are set at -450 and 0, respectively (number of levels = 16). The minimum and maximum horizontal displacement (u/L) contour levels are set at -0.005 and 0.005, respectively (number of levels = 11). The minimum and maximum vertical displacement (v/L) contour levels are set at -0.002 and 0.02, respectively (number of levels = 11). The same scale for the x and y co-ordinates is used in Plates 1(b)–4(d) (and y-thickness = L).

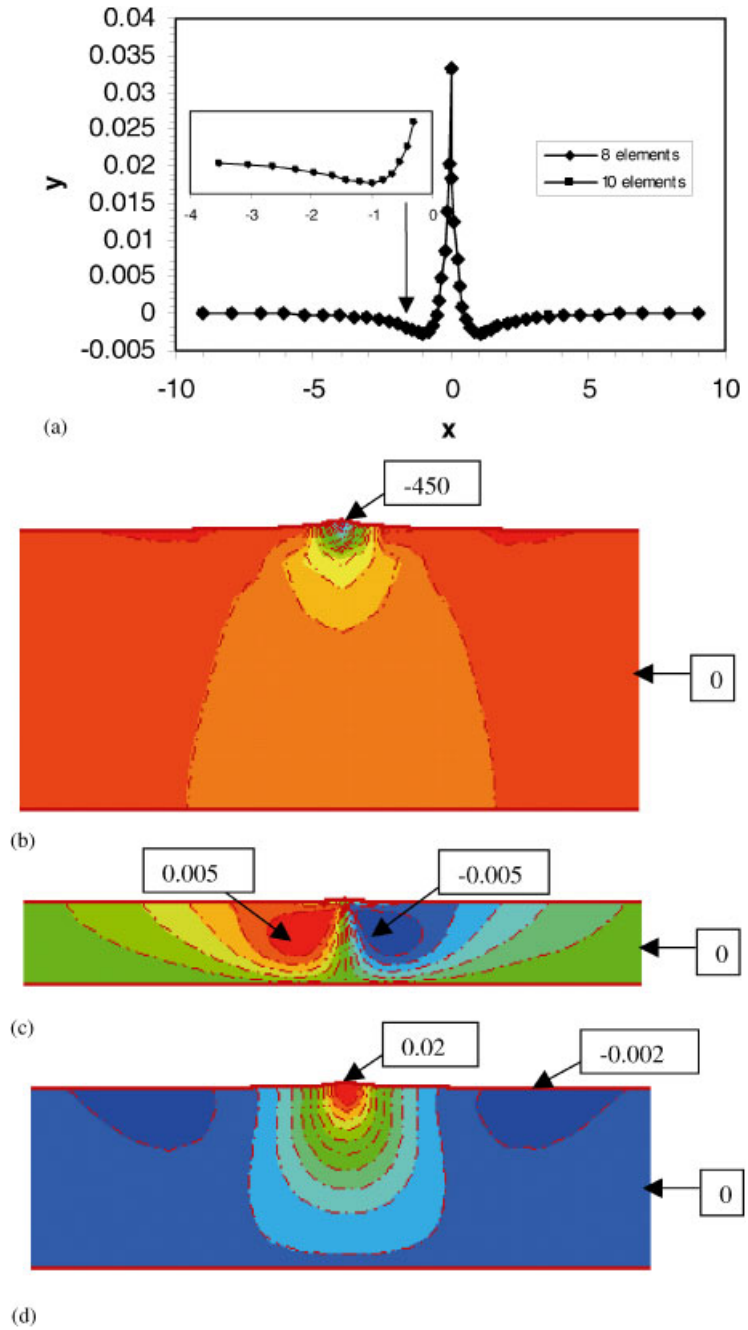

Plate 2. (a) Comparison of the free surface of the solid (co-ordinates x/L, y/L), with 8 elements versus 10 elements (in the y-direction). Comparison of contour plots of (b) pressure, (c) horizontal displacement and (d) vertical displacement, for 8 elements (solid areas) versus 10 elements (dash–dot lines). The same notations, values for parameters and the contour levels were used as in Plate 1.

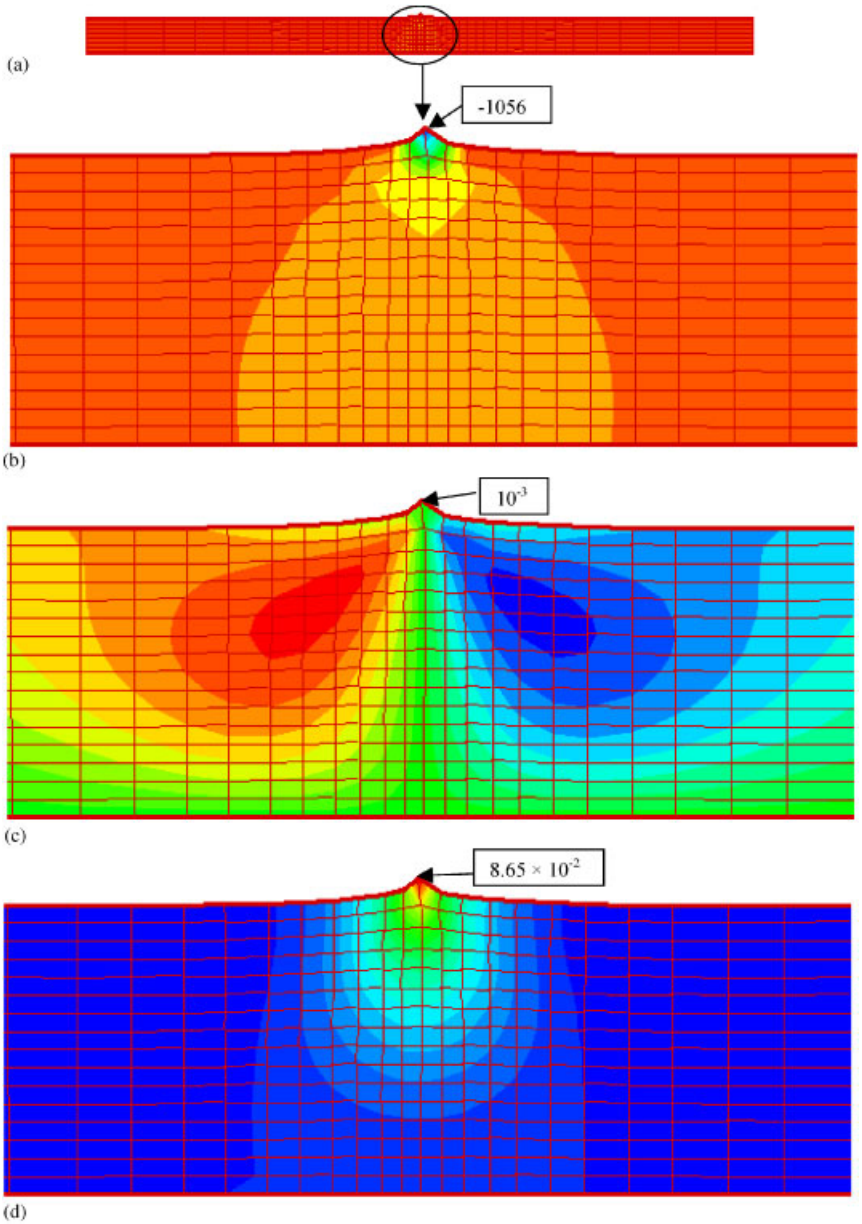

Plate 3. Contour plots of (a–b) pressure (the full domain is shown in (a)), (c) horizontal displacement and (d) vertical displacement, using the crease angle condition $\beta = 90^{\circ}$, and $\mathbf{Ca}_{\mathrm{ESV}} = \mathbf{Ca}_{\mathrm{ESL}} = 20$ ($f = 1$). The maximum and minimum pressure contour levels are at 50 and -1050, respectively (number of levels $= 12$), the value at the contact line being -1056. The maximum and minimum horizontal displacement contour levels are at 0.013 and -0.013, respectively (number of levels $= 14$), the value at the contact line being 10^{-3}. The maximum and minimum vertical displacement contour levels are at 0.08 and 0, respectively (number of levels $= 21$), the value at the contact line being 0.0865. Same scale along x and y, in Plates 1(b)–4(d) and y-thickness $= L$ in all the figures.

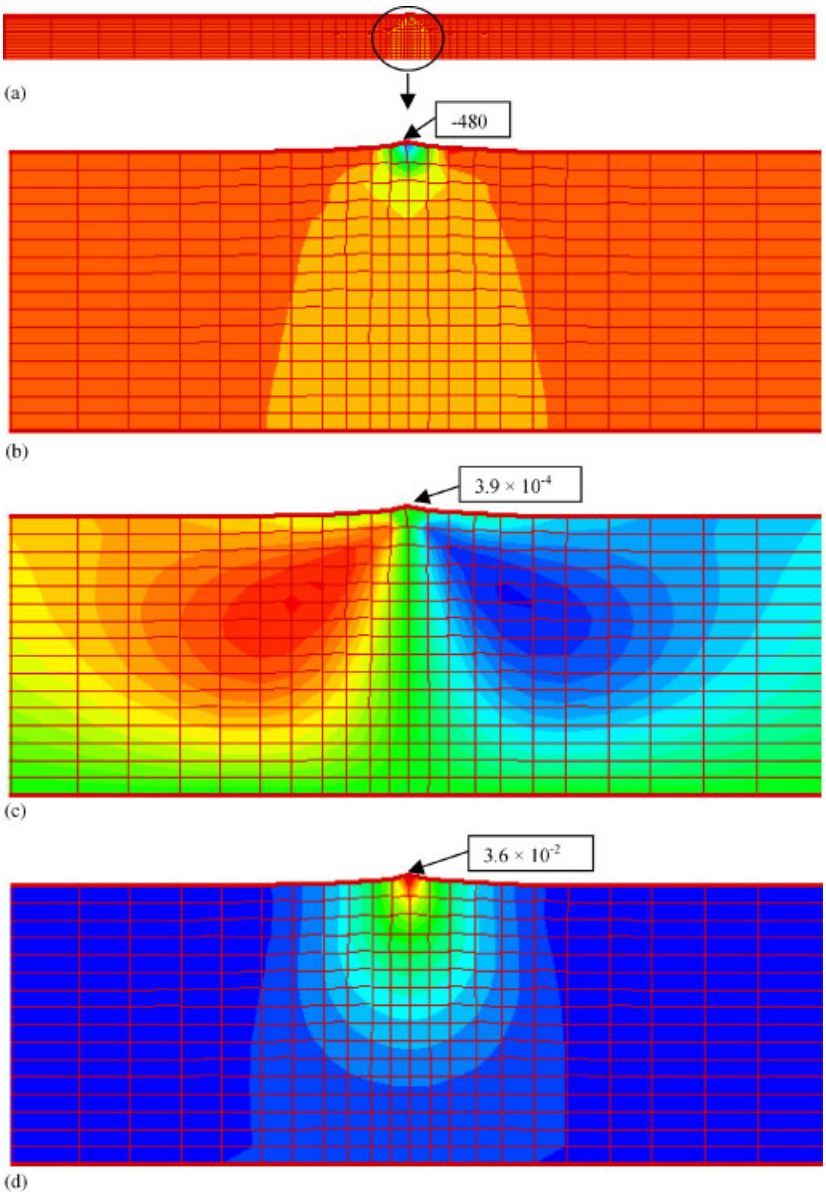

Plate 4. Contour plots of (a–b) with pressure (the full domain is shown in (a)), (c) horizontal displacement and (d) vertical displacement, using the distributed line force condition with $\mathbf{Ca}_{\mathrm{ELV}} = 14$ and $\mathbf{Ca}_{\mathrm{ESV}} = \mathbf{Ca}_{\mathrm{ESL}} = 20$ ($f = 1$). The maximum and minimum pressure contour levels are at 20 and -480, respectively (number of levels $= 11$), the value at the contact line being -480. The maximum and minimum horizontal displacement contour levels are at 0.006 and -0.006, respectively (number of levels $= 25$), the value at the contact line being 3.9×10^{-4}. The maximum and minimum vertical displacement contour levels are at 0.03 and 0, respectively (number of levels $= 16$), the value at the contact line being 0.036. Same scale along x and y, in Plates 1(b)–4(d) and y-thickness $= L$ in all the figures.

i.e. in dimensionless form (with co-ordinates x/L, y/L):

$$\int_{V_S} (\nabla \cdot \mathbf{T}_S)\phi_{SCL}\,\mathrm{d}V = -\int_{V_S} \mathbf{T}_S \cdot \nabla\phi_{SCL}\,\mathrm{d}V - \int_{S_{SL}} \frac{1}{\mathbf{Ca}_{ESL}} \nabla_s\phi_{SCL}\,\mathrm{d}S - \int_{S_{SV}} \frac{1}{\mathbf{Ca}_{ESV}} \nabla_s\phi_{SCL}\,\mathrm{d}S + \vec{\mathbf{m}}_{LV} \frac{1}{\mathbf{Ca}_{ELV}} \tag{21}$$

where $\mathbf{Ca}_{ELV} = GL/\sigma_{LV}$ is the elastic capillary number for the liquid/vapour surface.

3.3. Application of boundary conditions

In a two-dimensional model, Cauchy's equation of equilibrium results in two momentum residual components. The continuity equation is a scalar equation which determines pressure. The boundary conditions on the momentum equations are applied, either by adding the stress (second term in Equation (14)) to the momentum equation (weak form) or by replacing the entire momentum residual by the boundary condition, as a Dirichlet condition (strong form).

The capillary boundary conditions shown in (7)–(8) and the distributed line force condition are applied in the weak form. The rigid solid and rigid support boundary conditions (Figure 2(a)) and the crease angle condition are applied as Dirichlet conditions.

3.4. Method of solving the non-linear residual equations

The discretized equations resulting from applying the Galerkin FEM are a system of non-linear algebraic equations. These equations are linearized using the Newton's method [12, 18] and the resulting matrix is solved for updates of the variables, using a sparse solver [19]. The numerical integration is performed by Gaussian quadrature, using four Gauss points, in each direction. A structured mesh of quadrilateral elements with stretching is implemented. The elements are more concentrated and flattened (in the x-direction) near the contact node, their sizes being symmetrically arranged on both sides of the contact node.

3.5. Convergence test to determine the optimum number of elements

Mesh refinement was conducted to make the finite element solution independent of the mesh. The elements are more flattened (in the x-direction) towards the contact node, according to

$$\Delta x_1 = \frac{L_x}{2}\left(\frac{1-\eta}{1-\eta^{ne}}\right), \Delta x_2 = \eta\Delta x_1, \Delta x_3 = \eta\Delta x_2, \ldots, \Delta x_{ne} = \eta\Delta x_{ne-1}$$

where Δx_1 is the x-size of the first element (at the contact node), Δx_2 that of the second element and so on, L_x is the x-dimension of the solid domain, ne half the number of elements in the x-direction, and η the stretching parameter. For $\eta > 1$, the sizes increase, from the first element to the last one. In the following, dimensionless co-ordinates (x/L, y/L) and displacements ($u/L, v/L$) will be used.

The criterion for convergence is that the free surface shape of the solid for distance greater than about $0.5\,L$ to be insensitive to mesh refinement. This criterion is chosen because the outer solution (i.e. deformation at a distance greater than $0.5L$) is more relevant for macroscopic static wetting problems. Hence, it is expected that for converged solution with mesh

Table I. Convergence test for mesh refinement, with different number of elements in x-direction. Parameters $L_x/L = 18$, $f = 1$, $\beta = 150^\circ$ and $\mathbf{Ca}_{\mathrm{ESV}} = \mathbf{Ca}_{\mathrm{ESL}} = 10$. The reported element size is that of the element to the left of the contact line.

Number of elements ($x \times y$)	Size of the smallest element ($\Delta x \times \Delta y$)	Vertical displacement of contact node
12×8	0.7378×0.125	0.0658714
16×8	0.403×0.125	0.0487248
20×8	0.2308×0.125	0.0389942
24×8	0.1356×0.125	0.0332679
28×8	0.0808×0.125	0.0298642
32×8	0.0485×0.125	0.0278943
36×8	0.0293×0.125	0.0268415
40×8	0.0177×0.125	0.0263328

refinement, the outer solution does not change significantly. Furthermore, mesh refinement *cannot* converge with the distributed line force condition (as seen from Equation (23)); it will only converge if the element sizes adjacent to the contact node are held constant as shown in Reference [10]. Hence, the crease angle boundary condition is used for the convergence test. The tests are performed for the case of $L_x/L = 18$, $f = 1$, crease angle of 150° and solid/liquid and solid/vapour elastic capillary numbers of 10. First, the number of elements in the x-direction is changed, keeping that in the y-direction constant. Plate 1(a) shows that the free surface shapes, when the elements in the x-direction are changed from 16 to 24 elements and then to 28 elements, are almost the same. Plates 1(b)–1(d) compare the contours for pressure, horizontal displacement and vertical displacement, respectively, for 24 elements versus 28 elements, and they almost match up with each other. Moreover, Table I shows that there is a small change, i.e. of the order of 10^{-3}, in the predicted vertical displacement of the contact line, for a change of elements from 24×8 to 40×8 in the domain. From the above study, it can be concluded that 24 elements in the x-direction is the optimum number of elements, for convergence. On the right side of the contact line (or vapour side; see Figure 2(a) and 2(b)), η is set to 1.27, which gives $\Delta x_1 = 0.1463$ (at the contact node). On the left side (or liquid side), similar value $\eta = \frac{1}{0.78}$ is chosen, leading to $\Delta x_1 = 0.1356$.

The next step is to keep the number of elements in the x-direction constant and change that in the y-direction. Plate 2 shows that changing the number of elements from 8 to 10, there is negligible change in the free surface shape, contours of pressure, horizontal displacement and vertical displacement. The change in the vertical displacement of the contact line was of the order of 10^{-4}, when the number of elements was changed from 24×8 to 24×10, as shown in Table II. Hence, from the above study, eight elements are chosen in the y-direction.

4. RESULTS AND DISCUSSION

4.1. Finite element solution for the base case

The base case for the finite element solution is chosen to be $f = 1$, $\beta = 150^\circ$, $\mathbf{Ca}_{\mathrm{ESV}} = \mathbf{Ca}_{\mathrm{ESL}} = 10$ (and $L_x/L = 18$, for all numerical solutions). Plates 1 and 2 show the contours of pressure and displacements, for the base case. The pressure decays to zero rapidly, away from the

Table II. Convergence test for mesh refinement, with different number of elements in y-direction $\beta = 150^\circ$, and $\mathbf{Ca}_{\mathrm{ESV}} = \mathbf{Ca}_{\mathrm{ESL}} = 10$. The same parameters and notations were used as in Table I.

Number of elements ($x \times y$)	Size of the smallest element ($\Delta x \times \Delta y$)	Vertical displacement of contact node
24×2	0.1356×0.5	0.0384879
24×4	0.1356×0.25	0.0347414
24×6	0.1356×0.166	0.033697
24×8	0.1356×0.125	0.0332679
24×10	0.1356×0.1	0.0330376

contact line. At the contact line, the pressure is negative because the solid is in tension. The vertical displacement is a maximum at the contact node, because of the chosen crease angle. The horizontal displacement is non-zero at the contact node, due to unequal element sizes on either side of the contact line. The element size on the liquid side is smaller and hence, the stress is higher, which pushes the contact node to the vapour side. The horizontal displacement is positive on liquid side of contact line and negative on gas side (i.e. towards the contact line). The dip seen in Plate 1(a) or 2(a), on either side of the contact line, is due to the incompressibility constraint. The solid free surface asymptotically approaches a stress free condition, at distances far away from the contact line.

4.2. Analytical models of stress near the contact line

4.2.1. Singularity at the static wetting line. In a continuum approximation, liquid/vapour surface tension force acts on a line of the solid surface acts. At the contact line, infinite stress and displacement result, because of finite force acting over infinitesimal area, leading to non-physical results. Timoshenko and Goodier [20], and others, showed the variation of stress and displacement with the distance from the line of application. But, in reality, the force acts over a finite contact region of molecular dimensions, which relieves the singularity and results in finite stress and displacement. In the present FEM solution (with the distributed line force condition), force is effectively distributed over a contact region, which corresponds to the two elements adjacent to the contact node. Note that such a contact region, with x-size $(0.1356 + 0.1463)L = 0.2819L$, is of macroscopic (and not molecular) dimensions. The following section gives an analytical solution of the displacement, for a force distributed over a contact region.

4.2.2. Displacement field due to a distributed load. A semi-infinite solid is subjected to the normal force P (per unit length along the z-direction; see Figure 4), distributed over a contact region of finite extension $2a$, with a uniform pressure load q:

$$q = \frac{P}{2a} \tag{22}$$

The vertical displacement, at the mid-point of the contact region, is [20]

$$v = \frac{-q(2a \ln a)}{2\pi G} = -\frac{P \ln a}{2\pi G} \tag{23}$$

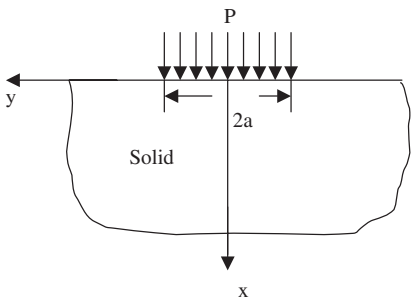

Figure 4. Force P (per unit length along z-direction) acting over a semi-infinite solid, and distributed over a contact region of finite extension $2a$.

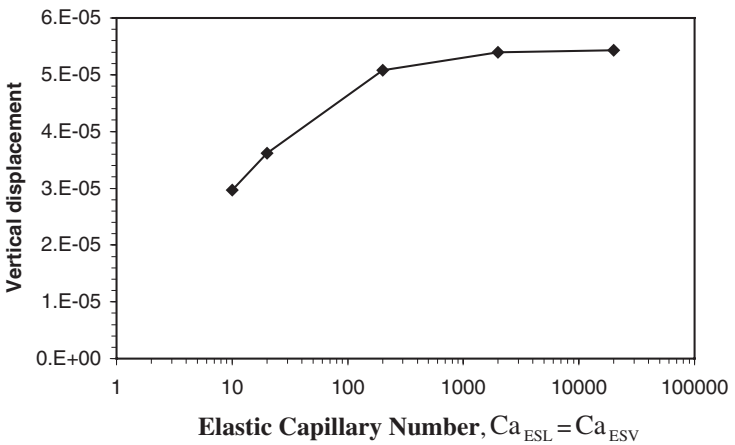

Figure 5. Vertical displacement of the contact line, as a function of solid/liquid or solid/vapour elastic capillary number, at $f = 1$ and $\mathbf{Ca}_{\mathrm{ELV}} = 1.4 \times 10^4$ (distributed line force condition).

(see Appendix A, for the derivation). Note that this vertical displacement is finite (and becomes infinite as $a \to 0$). Nevertheless, there is an ambiguity in Equation (23), since $\ln a$ is in fact $\ln a/R$, where R is an arbitrary constant length (see Appendix A).

4.3. Effect of elastic capillary number on vertical displacement of the contact line

The vertical displacement of the contact line is not a strong function of the solid/vapour or the solid/liquid elastic capillary numbers, using the distributed line force condition, as seen from Figure 5. The vertical displacement attains a constant value, at lower values of the solid/liquid or solid/vapour surface tension. The magnitude of the vertical displacement is mostly affected by the liquid/vapour surface tension (see Figure 9), as this force acts in the normal direction to the solid surface.

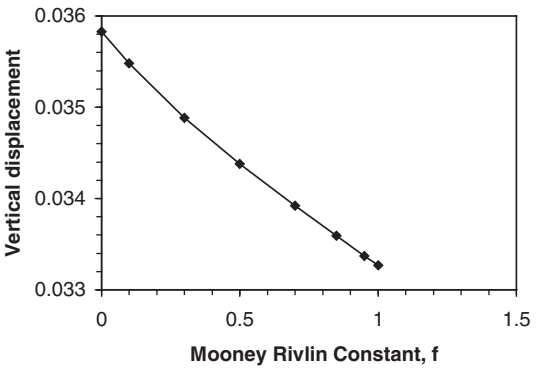

Figure 6. Vertical displacement of the contact line, as a function of parameter f, at $\beta = 150^\circ$ (crease angle condition), and $\mathbf{Ca}_{\mathrm{ESV}} = \mathbf{Ca}_{\mathrm{ESL}} = 10$.

4.4. *Effect of Mooney–Rivlin constant on vertical displacement of the contact line*

The effect of parameter f on the contact line displacement, has been studied at $\beta = 150^\circ$ (crease angle condition), $\mathbf{Ca}_{\mathrm{ESV}} = \mathbf{Ca}_{\mathrm{ESL}} = 10$. The results (Figure 6) show that the parameter f does not have a significant effect (relative change of around 7% with respect to $f = 1$) on the displacement, although the displacement is increasing with decrease in parameter f. Hence, the value of f is chosen to be 1 for all the following parametric studies. For vulcanized natural rubber, the value $f = 0.875$ was used by several researchers in the past [21, 22].

4.5. *Comparison of crease angle and distributed line force conditions*

At the contact line on a rigid solid, Neumann's triangle law of forces, applied to the three surface tensions, is not valid for the normal component: indeed, the normal elastic force, f_{sn}, is needed, according to Equation (2b). In this section, the two boundary conditions, namely, distributed line force and crease angle, are compared to show that normal component of Neumann's triangle law of forces, for the three surface tensions, is probably also not valid for flexible substrates.

We consider the following case: $\mathbf{Ca}_{\mathrm{ESV}} = \mathbf{Ca}_{\mathrm{ESL}} = 20$ (and $f = 1$). With the crease angle condition, we take $\beta = 90^\circ$, and, with the distributed line force condition, $\mathbf{Ca}_{\mathrm{ELV}} = 14$, i.e. $\sigma_{\mathrm{LV}} = \sqrt{2}\sigma_{\mathrm{SV}}$ (with $G = 10^4$ Pa and $L = 10^{-4}$ m, this leads to $\sigma_{\mathrm{LV}} = 0.07\ \mathrm{J\,m^{-2}}$, the water/air surface tension). This last value would be that of σ_{LV}, for $\beta = 90^\circ$, if Neumann's triangle law of forces, for the three surface tensions, were valid (Equation (2b) with $\theta = 90^\circ$, $\alpha = 45^\circ$ and $f_{\mathrm{sn}} = 0$).

Plates 3–4 compare the pressure and displacement fields, for these two conditions. With the distributed line force condition, the crease angle is 138.29°, which clearly differs from 90°. The full Newton iteration converges for a crease angle above 145°, (Continuation of Newton's method, where the solution at one set of conditions is used as an initial guess to the next set of conditions, can be used to go down as low as 30°). In addition, the magnitudes of the pressure and the displacements are different, for the two conditions. Then, if the action of the liquid/vapour surface tension is correctly modelled with the distributed line force condition (although it is distributed over a macroscopic and not molecular thickness),

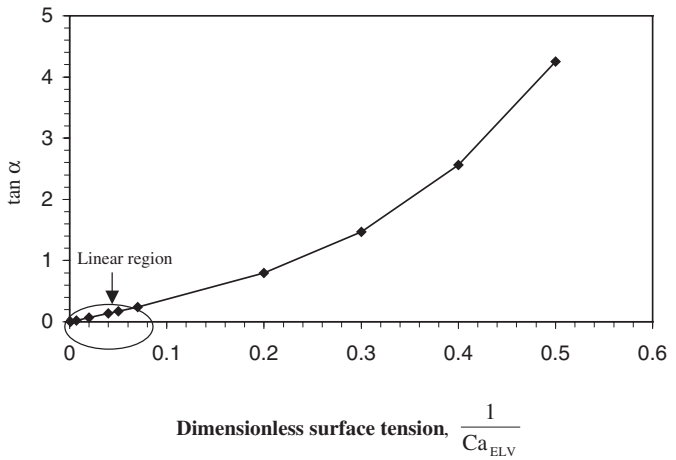

Figure 7. Angle α (rotation of the solid/liquid and solid/vapour interfaces) as a function of $1/\mathbf{Ca}_{\mathrm{ELV}}$, at $\mathbf{Ca}_{\mathrm{ESV}} = \mathbf{Ca}_{\mathrm{ESL}} = 10$ (distributed line force condition; $f = 1$).

the normal component of Neumann's triangle law of forces, for the three surface tensions, is probably not valid for flexible solids.

4.6. Angle α as a function of shear modulus and surface tension

Lester [3] gave the following relationship between α, Young's modulus and surface tension:

$$\alpha = \tan^{-1}\left(\frac{4\sigma_{\mathrm{LV}}(1-\upsilon^2)}{\pi\xi ER}\right) \tag{24}$$

where v is the Poisson's ratio, E the Young's modulus, R the radius of curvature of the liquid/vapour interface and ξ the ratio thickness of interface to the radius of droplet. Thus, $\xi R = 2a =$ thickness of liquid/vapour interface with $E = 3G$, $v = 0.5$ (neo-Hookean law, small strain, incompressible), and $2a/L = (0.1356 + 0.1463) = 0.2819$ (see Section 4.2 and Appendix A), it gives

$$\tan\alpha = \frac{1}{\pi(2a/L)\mathbf{Ca}_{\mathrm{ELV}}} = 1.13[\mathbf{Ca}_{\mathrm{ELV}}]^{-1} \tag{25}$$

The angle α is a function of shear modulus and liquid/vapour surface tension, as shown in Figure 7. The tangent of α is a linear function of inverse of liquid/vapour elastic capillary number, at lower values of α, but with a slope of 2.86, higher than the value of 1.13 of Equation (25). This may be due to uniform distribution of surface tension over the contact region of thickness $2a$ (Equation (23)), whereas, in the distributed line force condition (Figure 7), there is a non-uniform distribution, i.e. over a smaller 'effective contact region'. In addition, the relation deviates from linearity at smaller values of $\mathbf{Ca}_{\mathrm{ELV}}$, which could be due to the assumption of small strain (linearity), in Lester's [3] analysis.

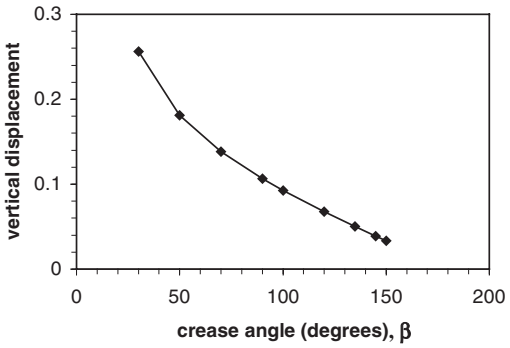

Figure 8. Vertical displacement of the contact line as a function of crease angle, at $\mathbf{Ca}_{\mathrm{ESV}} = \mathbf{Ca}_{\mathrm{ESL}} = 10$ (Crease angle condition; $f = 1$).

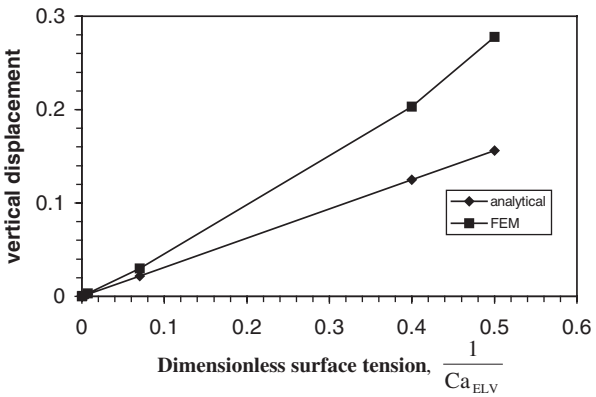

Figure 9. Vertical displacement of the contact line as a function $\mathbf{Ca}_{\mathrm{ELV}}$, for analytical model versus FEM, at $\mathbf{Ca}_{\mathrm{ESV}} = \mathbf{Ca}_{\mathrm{ESL}} = 10$ (distributed line force condition; $f = 1$).

4.7. Effect of crease angle

The vertical displacement is a strong function of the crease angle β (and of angle α, since $2\alpha + \beta = 180^\circ$), as seen in Figure 8. As the crease angle is decreased, the vertical displacement increases. It is possible that vertical displacement goes to infinity at crease angle of zero.

4.8. Comparison of analytical model and FEM

There is an ambiguity in the analytical model, due to the arbitrary constant length R, in the logarithm terms, such as r/R (see Section 4.2.2 and Appendix A). Nevertheless, if the value $R = L$ is chosen, the vertical displacement for varying liquid/vapour elastic capillary number, determined from the analytical model (Equation (A7) of Appendix A) compares qualitatively well with the predictions of the FEM, as shown in Figure 9, but quantitatively the solution from the analytical model is smaller. As in Section 4.6, one source of discrepancy is that, at large surface tension, FEM solution deviates from linearity (large strain elasticity), whereas

the analytical model is linear (small strain). Another discrepancy is that analytical model assumes the surface tension is distributed uniformly over the contact region of thickness $2a$ ($=0.2819L$; see Section 4.6 and Equation (A7)), whereas in FEM, the surface tension is non-uniformly distributed i.e. over a smaller 'effective contact region'.

5. CONCLUSIONS

This paper presents a finite element formulation to model static wetting on flexible substrates (with angle of contact $\theta = 90°$, and $\sigma_{SV} = \sigma_{SL}$). There is a singularity arising at the contact line due to the line force. Two boundary conditions were explored to relieve the singularity, namely, crease angle condition and distributed line force condition over a finite contact region (of macroscopic thickness; in reality, the surface tension acts on a contact region of molecular dimensions). It is known, from analytical models, that the line force acting on solid results in infinite displacement, whereas applying a distributed force over a finite contact region leads to a finite displacement. These numerical approaches suggest that normal component of Neumann's triangle law of forces, for the three surface tensions, is not valid for flexible substrates (as for rigid ones). The liquid/vapour elastic capillary number has a significant impact on the displacement of the contact line, unlike the solid/vapour or solid/liquid elastic capillary numbers. With decrease in liquid/vapour elastic capillary number, this displacement decreases increases and the crease angle decreases. The effect of the parameter f (of Mooney–Rivlin constitutive law) on the displacement is small. The FEM solution is in good qualitative agreement with comparable analytical solutions (although these ones present some ambiguities). Quantitative discrepancies may be due to (i) non-linearity and (ii) 'smaller effective contact region', in FEM.

The formulation could be a great asset to the coating industry, where many coating methods such as slot coating, slide coating, etc. involve static wetting at corners. The results give an idea of the order of displacements observed in flexible solids under static and equilibrium conditions, which could be useful information for performing experiments on contact angle and crease angle. The model developed in this paper has been extended to study dynamic wetting on flexible substrates [10].

APPENDIX A

The displacement field for a distributed load of intensity q acting over a finite contact region, as shown in Figure 4, is obtained by superposing the solutions for cases I and II shown in Figure A1. For case I, normal stresses $A\pi$ and $-A\pi$, respectively, act on the left side and the right side of the origin O, and a shear stress $-A$ on the whole surface. The corresponding Airy stress function ϕ [20] and the stress field are

$$\phi = Ar^2\theta \tag{A1}$$

$$\sigma_r = \frac{1}{r}\frac{\partial \phi}{\partial r} + \frac{1}{r^2}\frac{\partial^2 \phi}{\partial \theta^2} = 2A\theta$$

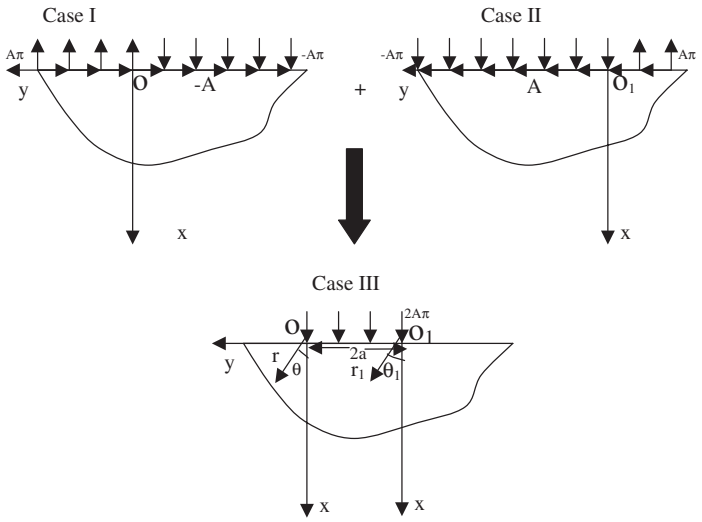

Figure A1. Pressure of magnitude $2A\pi$ acting on a semi-infinite solid, over a finite extension $2a$, between the two lines O_z and O_{1z}. r and θ are the polar co-ordinates with respect to O, r_1 and θ_1 those with respect to O_1.

$$\sigma_\theta = \frac{\partial^2 \phi}{\partial r^2} = 2A\theta \tag{A2}$$

$$\tau_{r\theta} = -\frac{\partial}{\partial r}\left(\frac{1}{r}\frac{\partial \phi}{\partial \theta}\right) = -A$$

Indeed, the value of σ_θ is $A\pi$ for $\theta = \Pi/2$, and $-A\pi$ for $\theta = -\Pi/2$.

For case III, the load intensity is $q = 2A\pi$, so that

$$A = \frac{q}{2\pi} \tag{A3}$$

The Airy stress function for case II is the same as that of case I, but with a negative sign, as the stresses are acting in opposite direction. For case I, the displacement field can be obtained by assuming linear neo-Hookean elasticity, small strain and incompressibility condition. In the region $y < 0$ of the surface (right side of the origin O), the horizontal (y-component) and vertical (x-component) displacements are, respectively:

$$\begin{aligned} u &= 0 \\ v &= \frac{-q(r \ln r)}{2\pi G} \end{aligned} \tag{A4}$$

The displacement for case II, in the region $y > -2a$ of the surface, is given by the same. The displacement for case III, in between two points O and O_1, is obtained by superposing the

displacements for cases I and II:

$$u = 0$$
$$v = \frac{-q(r \ln r + r_1 \ln r_1)}{2\pi G} \tag{A5}$$

For the mid-point between O and O_1, the displacement field is then

$$v = \frac{-q(2a \ln a)}{2\pi G} \tag{A6}$$

Nevertheless, there is an ambiguity in Equations (A4)–(A6), since each logarithm, say $\ln r$, is in fact $\ln r/R$, where R is an arbitrary constant length. For comparing with the finite element solution, $r = 0.1356$ and $r_1 = 0.1463$ are the element sizes (divided by L), respectively, upstream and downstream of the contact node. For example, by choosing the value $R = L$, Equation (A5) gives the following displacement (divided by L) of the contact node:

$$v = \frac{\sigma_{LV}(0.1356 \ln(0.1356) + 0.1463 \ln(0.1463))}{2\pi G(0.1356 + 0.1463)} = \frac{0.311}{\mathbf{Ca}_{ELV}} \tag{A7}$$

ACKNOWLEDGEMENTS

We are thankful to Sandia National Laboratories for financial support for this project and to the reviewers for helpful and extensive comments.

REFERENCES

1. Kistler SF, Schweizer PM. *Liquid Film Coating.* Chapman & Hall: London, 1997.
2. Berg JC. *Wettability.* Marcel Dekker: New York, 1993.
3. Lester GR. Contact angles of liquids at deformable solid surfaces. *Journal of Colloid Science* 1961; **16**:315–326.
4. Rusanov AI. Theory of the wetting of elastically deformed bodies. 1. Deformation with a finite contact angle. *Colloid Journal of the USSR* 1975; **37**:614.
5. Fortes MA. Deformation of solid surfaces due to capillary forces. *Journal of Colloid Interface Science* 1984; **100**:17–26.
6. Shanahan MER. Contact angle equilibrium on thin elastic solids. *Journal of Adhesives* 1985; **18**:247–267.
7. Kern R, Muller P. Deformation of an elastic thin solid induced by a liquid droplet. *Surface Science* 1992; **264**:467–494.
8. Olives J. Capillarity and elasticity. The example of the thin plate. *Journal of Physics-Condensed Matter* 1993; **5**:2081–2094.
9. Olives J. A combined capillarity and elasticity problem for a thin plate. *SIAM Journal of Applied Mathematics* 1996; **56**:480–493.
10. Madasu S, Cairncross RA. Effect of substrate flexibility on dynamic wetting: a finite element model. *Computer Methods in Applied Mechanics and Engineering* 2003; **192**:2671–2702.
11. Beatty MF. Topics in finite elasticity: hyperelasticity of rubber, elastomers, and biological tissues-with examples. *Applied Mechanics Reviews* 1987; **40**:1699–1734.
12. Sackinger PA, Schunk PR, Rao RR. A Newton–Raphson pseudo-solid domain mapping technique for free and moving boundary problems: a finite element implementation. *Journal of Computational Physics* 1996; **125**:83–103.
13. Chen KS, Schunk PR, Sackinger PA. Finite element analysis of blade and slot coating flows using a Newton–Raphson pseudo solid domain mapping technique and unstructured grids. *Coating Fundamentals Symposium Proceedings*, TAPPI Press: Atlanta, 1995; 131–152.
14. Cairncross RA, Schunk PR, Baer TA, Rao RR, Sackinger PA. A finite element method for free surface flows of incompressible fluids in three dimensions. Part I. Boundary fitted mesh motion. *International Journal for Numerical Methods in Fluids* 2000; **33**:375–403.

15. Baer TA, Cairncross RA, Schunk PR, Rao RR, Sackinger PA. A finite element method for free surface flows of incompressible fluids in three dimensions. Part II. Dynamic wetting lines. *International Journal for Numerical Methods in Fluids* 2000; **33**:405–427.
16. Oden JT, Carey GF. *Finite Elements*, *Mathematical Aspects.* vol. IV. Prentice-Hall: New Jersey, 1983.
17. Hanumanthu R. Patterned roll coating. *Ph.D. Dissertation*, University of Minnesota, Minneapolis, 1996.
18. Christodoulou KN, Scriven LE. The fluid mechanics of slide coating. *Journal of Fluid Mechanics* 1989; **208**: 321–354.
19. Kundert KS, Vincentelli AS. *A sparse linear equation solver*, *Version 1.3a*, University of California, Berkeley, 1988.
20. Timoshenko S, Goodier JN. *Theory of Elasticity*. McGraw-Hill: New York, 1951.
21. Ogden RW, Chadwick P. On the deformation of solid and tubular cylinders of incompressible isotropic elastic material. *Journal of the Mechanics and Physics of Solids* 1972; **20**:77–90.
22. Anand L. Moderate deformations in extension-torsion on incompressible isotropic elastic materials. *Journal of the Mechanics and Physics of Solids* 1986; **34**:293–304.

